Role of the Structural Domain of Troponin C in Muscle Regulation: NMR Studies of Ca^{2+} Binding and Subsequent Interactions with Regions 1−40 and 96−115 of Troponin I†

Pascal Mercier, Monica X. Li, and Brian D. Sykes*

MRC Group in Protein Structure and Function, Department of Biochemistry, University of Alberta, Edmonton, Alberta, Canada T6G 2H7

Received November 8, 1999; Revised Manuscript Received December 20, 1999

ABSTRACT: The interaction between the calcium binding and inhibitory components of troponin is central to the regulation of muscle contraction. In this work, two-dimensional heteronuclear single-quantum coherence nuclear magnetic resonance (2D-{^{1}H,^{15}N}-HSQC NMR) spectroscopy was used to determine the stoichiometry, affinity, and mechanisms for binding of Ca^{2+} and two synthetic TnI peptides [TnI_{1-40} (or Rp40) and TnI_{96-115}] to the isolated C-domain of skeletal troponin C (CTnC). The Ca^{2+} titration revealed that 2 equiv of Ca^{2+} binds to sites III and IV of CTnC with strong positive cooperativity and high affinity [dissociation constant (K_D) ≤ 0.1 μM]. In this process, CTnC folds from a largely unstructured state to a compact domain capable of interacting with TnI. Titration of CTnC·2Ca^{2+} with Rp40 occurs with a 1:1 stoichiometry and a K_D of 2 ± 1 μM. Titration of CTnC·2Ca^{2+} with a peptide corresponding to the inhibitory region of TnI (TnI_{96-115}) also reveals a 1:1 ratio, but weaker affinity (K_D = 47 ± 7 μM). Both Rp40- and TnI_{96-115}-induced backbone amide chemical shift changes of CTnC·2Ca^{2+} are similarly distributed along the sequence, indicating that these two regions of TnI may compete for the same binding site on CTnC·2Ca^{2+}. The changes induced by Rp40 are much larger, however, and define the interaction sites on TnC and regions where the flexibility of hinge and terminal residues is altered. To investigate the possibility of direct competition, TnI_{96-115} was titrated into the CTnC·2Ca^{2+}·Rp40 complex, whereas Rp40 was titrated into the CTnC·2Ca^{2+}·TnI_{96-115} complex. The results show that Rp40 can displace TnI_{96-115} completely, while TnI_{96-115} has no effect on CTnC·2Ca^{2+}·Rp40. Recent proposals for the mechanism of muscle regulation [Tripet, B. P., Van Eyk, J. E., and Hodges, R. S. (1997) *J. Mol. Biol. 271,* 728−750] suggest that the N-terminal and inhibitory regions of TnI competitively bind the structural domain of TnC. The findings presented here indicate that additional factors, such as interactions between the N-domain of TnC with the C-domain of TnI or the C-domain of TnT, are required, if the inhibitory region is going to successfully compete for the structural domain of TnC.

Muscle contraction is regulated by Ca^{2+} binding to the troponin complex which triggers a cascade of altered protein−protein interactions, leading to force development. The troponin complex is comprised of three components: troponin C (TnC),[1] TnI, and TnT. TnC responds to the Ca^{2+} signal, TnI inhibits interactions between thick and thin filaments in the absence of Ca^{2+}, and TnT anchors troponin to actin and transmits the Ca^{2+} signal along the thin filament, thereby enhancing the actomyosin ATPase activity (for reviews, see refs *1*−*6*).

TnC is a dumbbell-shaped molecule with two globular domains connected by a central linker (*7*−*11*). Each domain contains two metal binding sites, designated sites I and II in the N domain and sites III and IV in the C-domain, with each site consisting of two helix−loop−helix EF-hand motifs typical of calcium binding proteins (*12*). Sites III/IV are Ca^{2+}/Mg^{2+} sites, which are believed to be always occupied by either Ca^{2+} or Mg^{2+} in muscle cells, whereas sites I/II are Ca^{2+}-specific sites (see reviews listed above and refs *13*−*15*). While Ca^{2+}- or Mg^{2+}-bound C-domain anchors troponin to the thin filament, association and dissociation of Ca^{2+} from sites I/II (in the N-domain) triggers switching between muscle contraction and relaxation, respectively. The N-domain of TnC is composed of five α-helices and a short β-sheet and is structured in the apo state. Ca^{2+} binding to sites I/II is accompanied by a rearrangement of secondary structural elements such that helices B and C move as a unit relative to N, A, and D helices. As a result, a hydrophobic patch on the surface of the molecule is exposed, which has been shown to interact with TnI (for a review, see *16* and references cited therein). On the other hand, CTnC is largely unstructured,

†This work was supported by the Medical Research Council Group in Protein Structure and Function. P.M. is supported by the Natural Sciences and Engineering Research Council of Canada (studentship).

* To whom correspondence should be addressed. E-mail: brian.sykes@ualberta.ca, Phone: (780) 492-5460, Fax: (780) 492-0886.

[1] Abbreviations: TnC, troponin C; NTnC, N-domain (residues 1−90) of recombinant chicken skeletal TnC; CTnC, C-domain (residues 88−162) of recombinant chicken skeletal TnC; TnI, troponin I; TnT, troponin T; Rp40, N-terminal synthetic peptide (residues 1−40) of rabbit TnI; TnI_{96-115}, inhibitory synthetic peptide (96−115) of chicken skeletal TnI; NMR, nuclear magnetic resonance; HSQC, heteronuclear single-quantum coherence; HMQC, heteronuclear multi-quantum coherence.

10.1021/bi992579n CCC: $19.00
Published on Web 02/22/2000

and Ca^{2+} binding to sites III and IV leads to a structured globular domain with an exposed hydrophobic pocket (*16*). The replacement of Ca^{2+} by other metal ions, such as Mn^{2+}, Cd^{2+}, and Tb^{2+}, in sites III/IV has minimal effect on the globular fold of the domain, as revealed by the X-ray structures of Mn^{2+}, Cd^{2+}, and Tb^{2+} metal complexes of troponin C (*17*).

Since NTnC accomplishes a regulatory role while CTnC plays predominantly a structural role, the Ca^{2+} binding mechanisms for the two domains are distinct from each other. Previously, we performed a Ca^{2+} titration of NTnC using 2D-{^{1}H,^{15}N}-HMQC NMR spectroscopy (*18*). The results demonstrated that Ca^{2+} binding to the regulatory domain occurs in a stepwise manner with the Ca^{2+} affinity of one site being approximately 10-fold stronger than that of the other. We were able to assign the order of the stepwise binding as site II then site I by following Ca^{2+} binding to an E41A mutant of NTnC (*19*). The same approach has been used to investigate Ca^{2+} binding to cardiac TnC (*19*), calmodulin (CaM) (*20, 21*), and calbindin D_{9k} (*22*), as well as the interaction between TnC and TnI peptides (*23, 24*). This method is especially powerful since it can reveal information that pertains to individual atoms throughout the protein sequence.

While much is known about how Ca^{2+} induces structural changes in NTnC and initiates a cascade of protein−protein interactions leading to muscle contraction, less is known about TnI inhibition of actomyosin−ATPase. Neutron scattering studies have shed some light on the general aspects of the TnI·TnC interaction (*25, 26*). However, there are no high-resolution structures of the complex due in part to the low solubility of TnI. Several groups have used different synthetic fragments of TnI complexed with TnC (*23*−*39*) in order to identify the sites of interaction between TnI and TnC. Together, these studies provide information about the structure of the TnC·TnI complex and broaden knowledge regarding the inhibition of muscle contraction by TnI.

Considerable attention has been focused on the inhibitory region (residues 96−115) of TnI since it was first identified by Syska et al. (*40*). Studies by Talbot and Hodges (*41*) using synthetic peptides revealed that residues 104−115 represent the minimal sequence required for inhibition. Further studies with $TnI_{104-115}$ by Van Eyk and Hodges (*42*) suggested that the major switch between contraction and relaxation involves a movement of the inhibitory region of TnI from TnC to actin−tropomyosin, respectively. Farah and co-workers showed that TnC and TnI interact in an antiparallel fashion (*43*). Recent work by Tripet et al. further refined the binding organization of TnI to TnC, specifically with the N-terminal 1−40 and the inhibitory region 96−115 of TnI binding to the C-domain, the 40−96 region of TnI interacting with TnT and/or tropomyosin (*30*), the 115−131 region of TnI interacting with the N-domain of TnC, and the C-terminal region of TnI interacting with actin. Thus, the interactions between CTnC and the N-domain of TnI are critical for maintaining TnC in the ternary troponin complex (for a review, see *4*).

The location of binding sites for the inhibitory region of TnI on TnC has long been in dispute. Early chemical cross-linking studies (*44*−*50*) suggested that both the N- and C-domains of TnC are in close proximity to the inhibitory region of TnI and support the conclusion that TnC in the presence of TnI adopts a more compact conformation in solution than in its crystal structure. However, small-angle X-ray data indicate no such conformational change in TnC upon addition of TnI_{96-115} (*51*), and available neutron scattering studies in the presence of intact TnI (*25, 26*) or with the whole troponin complex (*52*) are consistent with an extended structure for TnC.

Structural studies of the inhibitory region include the NMR structure of $TnI_{104-115}$ in the TnC·4Ca^{2+}·$TnI_{104-115}$ complex (*31*) and a recent NMR and CD investigation of TnI_{96-115} in the TnC·4Ca^{2+}·TnI_{96-115} complex (*39*). By monitoring chemical shift perturbation, Campbell and Sykes (*31*) have suggested that $TnI_{104-115}$ interacts with the hydrophobic cleft in CTnC. Slupsky et al. (*34*) have reported similar findings for $TnI_{104-115}$ binding sites on a synthetic peptide heterodimer representing sites III/IV of the CTnC. Based on these results and photochemical cross-linking studies between TnC and $TnI_{104-115}$, Ngai et al. (*27*) constructed a model of CTnC·$TnI_{104-115}$ that indicates the $TnI_{104-115}$ structure determined by Campbell and Sykes (*31*) fits within the hydrophobic patch of CTnC.

A recent X-ray structure of skeletal TnC in complex with TnI_{1-47} showed that TnI_{3-33} forms a long α-helix that binds within the hydrophobic groove of CTnC as well (*53*). The corresponding region of cardiac TnI_{33-80} has also been shown to bind within the hydrophobic patch of the C-domain of cardiac TnC (*37*). Functional studies of this region by Ngai and Hodges (*54*) have shown that Rp40 can effectively compete with TnI or TnI inhibitory peptide (residues 96−115) for TnC, suggesting that the N-terminus of TnI may play both a structural and a functional role.

Based on the crystal structure of TnC·2Ca^{2+}·TnI_{1-47}, Maeda et al. (*53*) have proposed a model of interaction of TnC and TnI in which the central linker of TnC is unwound at its center. As a result, TnC would possess a more compact structure, allowing direct interactions between the N- and the C-domains. According to this model, the inhibitory region interacts with both the N- and C-domains of TnC even when the hydrophobic patch in CTnC is occupied by TnI_{1-47} (*53*). On the other hand, Tripet et al. (*30*) have proposed that Rp40 and TnI_{96-115} may bind to similar sites within CTnC but are regulated by other Ca^{2+}-dependent changes in the interaction between TnC and TnI. It was identified that the binding of $TnI_{116-131}$ to NTnC plays a key role in modulating the affinity between Rp40 and TnI_{96-115} for CTnC. Their results showed that in the absence of $TnI_{116-131}$, Rp40 dominates in affinity for TnC over TnI_{96-115}, whereas the affinity is reversed in the presence of $TnI_{116-131}$. Therefore, to release inhibition, the binding of $TnI_{116-131}$ to TnC is critical. In addition, Farah et al. (*43*) have suggested that residues 116−156 of TnI are responsible for the expression of maximum inhibition, in addition to the inhibitory region. Moreover, a recent paper by Ramos (*55*) suggested that the entire C-terminal region of TnI is necessary for the regulatory activity of TnI.

Despite structural and functional studies, there are no quantitative affinities and exact stoichiometries reported for Rp40 and TnI_{96-115} binding to TnC. In this paper, we have performed detailed titrations of Ca^{2+}, Rp40, and TnI_{96-115} binding to CTnC as monitored by 2D-{^{1}H, ^{15}N}-HSQC NMR spectroscopy. The titrations allow for the determination of binding constants, the stoichiometry, and the evaluation of competitive binding of Rp40 and TnI_{96-115} to CTnC. The

binding sites of Rp40 and TnI_{96-115} on CTnC are mapped following chemical shift changes upon peptide binding, and together with Ca^{2+} binding properties, this work provides insight into the role of the structural domain in muscle contraction.

EXPERIMENTAL PROCEDURES

Construction of CTnC Mutant and Protein Isolation. The engineering of CTnC (88−162) into the expression vector pET3a was as described for NTnC (1−90) (*56*) except for the use of two different oligonucleotides that are complementary to the sequence and restriction enzyme sites. The expression and purification of [^{15}N]-CTnC in minimal media follow the procedure as described for [^{15}N]-NTnC (*18*, *56*). During expression in *E. coli*, the N-terminal methionine, corresponding to the initiation codon, is not cleaved off.

Ca^{2+} Titration of [^{15}N]-CTnC. Decalcification of [^{15}N]-CTnC and NMR sample preparation were as described for [^{15}N]-NTnC (*18*). Since CTnC has higher affinity for Ca^{2+} than NTnC, the 25 mM $(NH_4)HCO_4$ buffer pH for the decalcification step was raised to 8.5. The solution conditions were 100 mM KCl, 10 mM imidazole, and 15 mM DTT in 90% H_2O/10% D_2O at pH 6.7 (uncorrected for ^{2}H isotope effects). The protein concentration was determined to be 0.9 mM by amino acid analysis in triplicate. All solutions used in this study were treated with Chelex 100 before use to remove metal contaminants. A stock solution of 50 mM $CaCl_2$ in 90% H_2O/10% D_2O was prepared from standardized 100 mM $CaCl_2$ in water. With a 10 μL Hamilton syringe, aliquots of 5 μL of stock $CaCl_2$ solution were added to the NMR tube (the volume of the NMR sample was 500 μL) for each titration point and mixed thoroughly. The total volume increase was 45 μL, and the change in protein concentration due to dilution was taken into account for data analysis. Changes in pH due to additions of stock $CaCl_2$ solution were negligible. Both 1D ^{1}H and 2D-{^{1}H, ^{15}N}-HSQC NMR spectra were acquired at every titration point.

Rp40 Titration of [^{15}N]-CTnC·2Ca^{2+}. Rp40 peptide, acetyl-GDEEKRNRAITARRQHLKSVMLQIAATELEKE-EGRREAEK-amide, was synthesized and purified as described in Ngai and Hodges (*54*). Since Rp40 peptide is not soluble in aqueous solution at concentrations needed for stock solutions, solid peptide was added to a 0.51 mM NMR sample of CTnC·2Ca^{2+}. Titration points of 0.1, 0.25, 0.35, 0.5, 0.7, 0.75, 0.85, 0.9, 1, 1.05, and 1.2 molar equiv of Rp40 were observed, consecutively. The initial concentration of CTnC·2Ca^{2+} and Rp40:CTnC ratios were determined by amino acid analyses in duplicate. Both 1D ^{1}H and 2D-{^{1}H, ^{15}N}-HSQC NMR spectra were acquired at every titration point. The pH was adjusted to 6.7 after each Rp40 addition.

TnI_{96-115} Titration of [^{15}N]-CTnC·2Ca^{2+}. The synthetic peptide TnI_{96-115}, acetyl-QKLFDLRGKFKRPPLRRVR-amide, was prepared and analyzed as by Tripet et al. (*30*). Two stock solutions of TnI_{96-115} of 20 and 50 mM were prepared in double-distilled water, respectively. Molar equivalents of 0.7, 0.15, 0.2, 0.3, 0.35, 0.40, 0.5, 0.55, 0.62, 0.7, 0.75, 0.8, 1.3, 2.0, and 2.7 of TnI_{96-115} were added to the NMR sample consecutively using 1.5 μL aliquots of the 20 mM solution for the first 12 points, one 4.8 μL aliquot of the 50 mM solution for the 13th point, and 6 μL aliquots of the 50 mM solution for the last 2 points. The initial concentration of [^{15}N]-CTnC was determined to be 0.80 mM by amino acid analysis in duplicate. Both 1D ^{1}H and 2D-{^{1}H, ^{15}N}-HSQC NMR spectra were acquired at every titration point.

Rp40 Titration of [^{15}N]-CTnC·2Ca^{2+}·TnI_{96-115}. Solid Rp40 peptide was added to an NMR sample containing [^{15}N]-CTnC·2Ca^{2+}·TnI_{96-115} following the same procedure for the titration of CTnC·2Ca^{2+} with Rp40. Molar equivalents of 0.2, 0.3, 0.4, 0.56, 0.7, 0.83, 0.98, and 1.2 of Rp40, as determined by amino acid analysis in duplicate, were added to the NMR sample, consecutively. The initial CTnC and TnI_{96-115} concentrations were determined to be 0.7 and 1.9 mM by amino acid analysis in duplicate (initial complex: 1 CTnC:2.7 TnI_{96-115}), respectively. Both 1D ^{1}H and 2D-{^{1}H, ^{15}N}-HSQC NMR spectra were acquired at every titration point.

TnI_{96-115} Titration of [^{15}N]-CTnC·2Ca^{2+}·Rp40. A TnI_{96-115} stock solution of 20 mM was prepared in double-distilled water. For the first eight titration points, 2 μL aliquots were added to an NMR tube containing [^{15}N]-CTnC·2Ca^{2+}·Rp40. The ninth addition was performed by adding a 12 μL aliquot, and the last two additions were performed by adding solid peptide directly to the NMR sample. The initial concentrations of [^{15}N]-CTnC and Rp40 were determined to be 0.51 and 0.61 mM, respectively, by amino acid analysis in duplicate. Amino acid analysis gave 0.15, 0.3, 0.45, 0.6, 0.75, 0.9, 1.05, 1.2, 2.1, 5.3, and 10.4 molar equiv of TnI_{96-115} to [^{15}N]-CTnC·2Ca^{2+}·Rp40, respectively. Both 1D ^{1}H and 2D-{^{1}H, ^{15}N}-HSQC NMR spectra were acquired at every titration point.

NMR Spectroscopy. All 1D ^{1}H and 2D-{^{1}H, ^{15}N}-HSQC NMR spectra were recorded on a Varian Unity INOVA 500 MHz spectrometer. The 1D ^{1}H NMR spectra were acquired using a spectral width of 6200 Hz, a ^{1}H pulse width of 10 μs (90°), and an acquisition time of 2.5 s. The 2D-{^{1}H, ^{15}N}-HSQC NMR spectra were acquired using the sensitivity-enhanced gradient pulse scheme developed by Lewis E. Kay and co-workers (*57*, *58*). The ^{1}H and ^{15}N sweep widths were 6200 and 1500 Hz, respectively. A minimum of 8 transients were acquired for each titration point. Processing of the data sets was accomplished using the VNMR software package (VNMR 5.3B, Varian, Palo Alto, CA) and the program NMRPipe (*59*).

RESULTS

Titration of [^{15}N]-CTnC with Ca^{2+}. Ca^{2+} binding to [^{15}N]-CTnC was followed by 2D-{^{1}H, ^{15}N}-HSQC NMR spectroscopy. The 2D-{^{1}H, ^{15}N}-HSQC NMR spectra of [^{15}N]-CTnC at the beginning of the titration (CTnC·apo) and the end of the titration (CTnC·2Ca^{2+}) are shown in Figure 1A and 1B, respectively. In the apo state, most of the amide resonances are located at the center of the plotted region with little dispersion in ^{1}H chemical shifts (Figure 1A). The peaks fall within regions of ^{1}H chemical shift characterized as "random coil" by Wüthrich (*60*). The ^{15}N chemical shifts also correspond to random coil values (*61*). These observations suggest that CTnC·apo does not adopt a defined structure in solution. The first Ca^{2+} addition (0.56:1 molar ratio) to CTnC results in dramatic changes in the 2D-{^{1}H, ^{15}N}-HSQC NMR spectra with the appearance of a new set

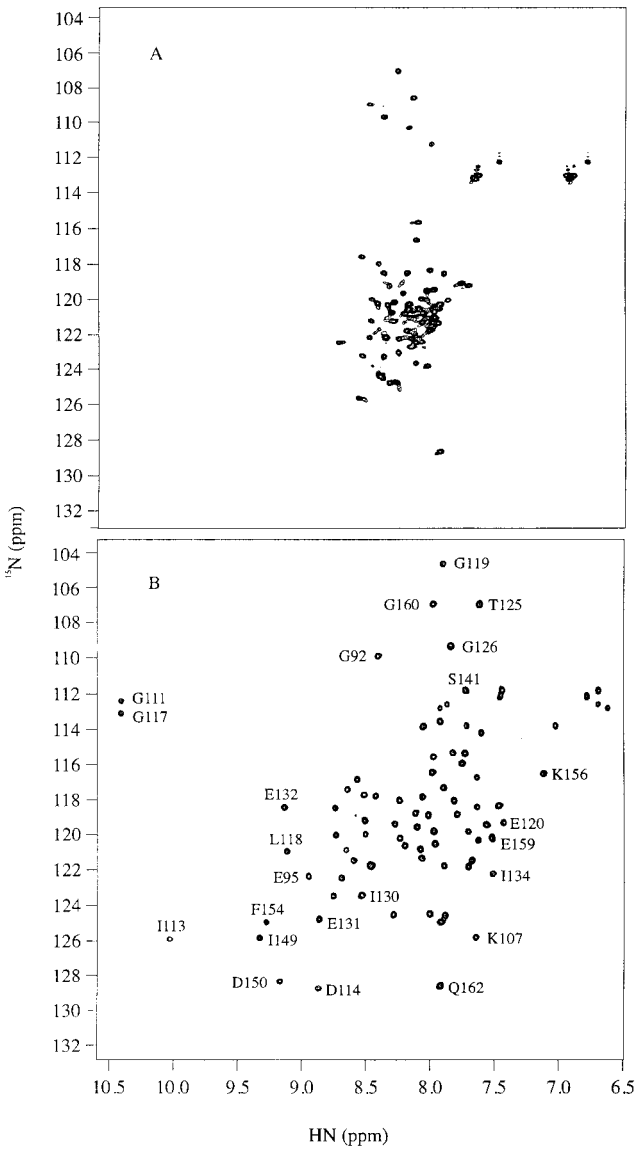

FIGURE 1: Titration of CTnC with Ca^{2+}. 500 MHz 2D-{^{1}H, ^{15}N}-HSQC NMR spectrum of CTnC. (A) In the apo state and (B) in the Ca^{2+}-saturated state (CTnC·$2Ca^{2+}$). Assignments for some residues are indicated.

of signals corresponding to CTnC·$2Ca^{2+}$. As the $[Ca^{2+}]_{total}$:$[CTnC]_{total}$ ratio is increased, these resonances increase in intensity with no line broadening throughout the entire titration until the spectrum shown in Figure 1B is obtained. Concomitantly, the resonances corresponding to CTnC·apo become less intense and completely disappear when the $[Ca^{2+}]_{total}$:$[CTnC]_{total}$ ratio reaches 2. The increased chemical shift dispersion indicates that CTnC is undergoing a Ca^{2+}-induced structural folding. The spectral changes are consistent with slow exchange kinetics on the NMR time scale, and further additions of Ca^{2+} generate no increase in signal intensity. These results indicate that the stoichiometry of Ca^{2+} binding to CTnC is 2:1, corresponding to binding of Ca^{2+} to sites III and IV. The 2D-{^{1}H, ^{15}N}-HSQC NMR spectrum of CTnC·$2Ca^{2+}$ (Figure 1B) was completely assigned with the exception of the first two N-terminal residues, which were not observed, likely due to rapid exchange with water. Ca^{2+} binding to CTnC was quantified by plotting the normalized intensity changes of each residue during the Ca^{2+} titration as a function of the $[Ca^{2+}]_{total}$:$[CTnC]_{total}$ ratio (Figure 2A). The curve in Figure 2A clearly shows that 2 equiv of Ca^{2+} is needed to saturate CTnC. The spectroscopic changes between 0 and 2 equiv of Ca^{2+} are linear, implying that sites III and IV in CTnC either have intrinsically identical Ca^{2+} binding sites or bind Ca^{2+} with strong positive cooperativity (*18*). Curve fitting using the equation:

$$P + Ca \underset{K_{D1}}{\rightleftharpoons} P{\cdot}Ca \underset{K_{D2}}{\rightleftharpoons} P{\cdot}Ca_2 \qquad (1)$$

corresponding to the Ca^{2+} binding equilibrium for a two-site protein yields macroscopic or stoichiometric dissociation constants of $K_{D1} \leq 0.1\ \mu$M and $K_{D2} \leq 0.42\ \mu$M. As pointed out by Ferguson-Miller and Koppenol (*62*), $K_{D2} = 4K_{D1}$ indicates that the intrinsic microscopic binding constants for the two sites are the same, and $K_{D2} > 4K_{D1}$ indicates positive cooperativity between the two sites. Since Ca^{2+}-induced changes on CTnC are uniform throughout the sequence, and any residue gives an identical curve as that shown in Figure 2A, it is extremely unlikely that the two Ca^{2+} binding sites are independent. The binding affinity for Ca^{2+} ($K_D \leq 0.1\ \mu$M) agrees with previously published constants (*1*−*3*).

Titration of CTnC·2Ca²⁺ with Rp40. Figure 3 shows a superimposition of the 2D-{^{1}H, ^{15}N}-HSQC NMR spectra of CTnC·$2Ca^{2+}$ and CTnC·$2Ca^{2+}$·Rp40. Similar to Ca^{2+} binding to CTnC, Rp40 binding to CTnC·$2Ca^{2+}$ occurs with slow exchange kinetics on the NMR time scale. Thus, as the titration progresses, the resonance peaks corresponding to CTnC·$2Ca^{2+}$ becomes less intense while those corresponding to CTnC·$2Ca^{2+}$·Rp40 grow. Line broadening is not observed. When the $[Rp40]_{total}$:$[CTnC{\cdot}2Ca^{2+}]_{total}$ ratio reaches 1, all cross-peaks corresponding to CTnC·$2Ca^{2+}$ completely disappear while those corresponding to CTnC·$2Ca^{2+}$·Rp40 attain maximum intensity. The normalized intensity changes of seven residues (C101, D106, S141, E159, G160, V161, and Q162) gave identical values at each titration point. The curve shown in Figure 2B shows the normalized intensity changes of the seven peaks with the $[Rp40]_{total}$:$[CTnC{\cdot}2Ca^{2+}]_{total}$ ratio calculated from two amino acid analyses. Curve fitting to the equation:

$$CTnC{\cdot}2Ca^{2+} + Rp40 \rightleftharpoons CTnC{\cdot}2Ca^{2+}{\cdot}Rp40 \qquad (2)$$

yields a K_D of $2 \pm 1\ \mu$M, indicating that Rp40 and CTnC·$2Ca^{2+}$ form a tight complex. This result quantitatively explains the enhanced interaction between the N-terminus of TnI and CTnC as observed in many biological and biophysical experiments [for a review, see Farah and Reinach (*4*)]. For instance, it was found that the complex between TnC and Rp40 is stable even in the presence of 6 M urea (*54*).

The CTnC residues perturbed by Rp40 binding were identified by plotting the total change in backbone amide ^{1}HN and ^{15}N chemical shifts for each resonance (see Figure 4A). The total change in chemical shift was calculated with the following equation adopted from McKay et al. (*23*):

$$\Delta_{total} = \sqrt{(\Delta\delta^{15}N)^2 + (\Delta\delta^{1}H)^2} \qquad (3)$$

where $\Delta\delta^{15}$N and $\Delta\delta^{1}$H are the chemical shift changes in hertz. Although Rp40 induces chemical shift changes for backbone amide ^{1}HN and ^{15}N of CTnC·$2Ca^{2+}$ throughout

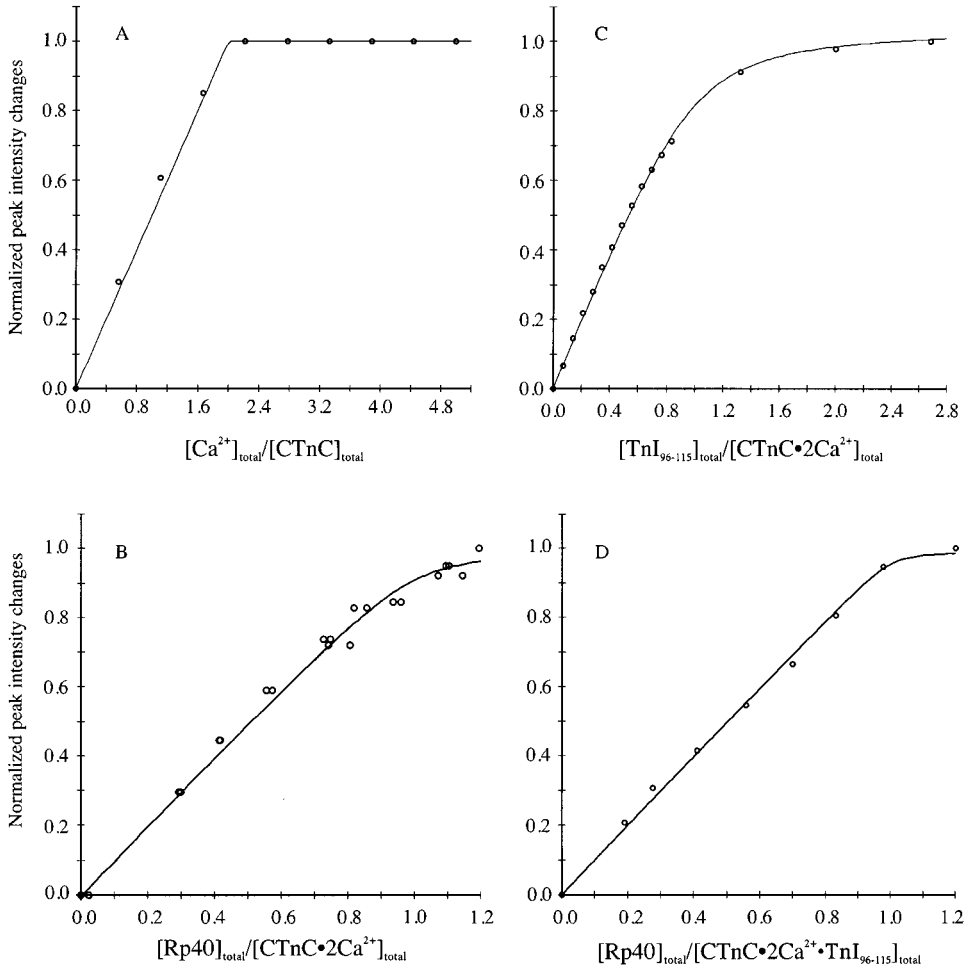

FIGURE 2: Binding curves obtained from the averaged normalized peak intensity changes in the 2D-{^{1}H, ^{15}N}-HSQC NMR spectrum of (A) CTnC during titration with Ca^{2+} ($K_D \leq 0.1$ μM), (B) CTnC·$2Ca^{2+}$ during titration with Rp40 ($K_D = 2 \pm 1$ μM), (C) CTnC·$2Ca^{2+}$ during titration with TnI_{96-115} ($K_D = 47 \pm 7$ μM), and (D) CTnC·$2Ca^{2+}$·TnI_{96-115} during titration with Rp40 ($K_D = 3 \pm 1$ μM). In (B), because of slight variance in the $[Rp40]_{total}$:$[CTnC{\cdot}2Ca^{2+}]_{total}$ ratios calculated from amino acid analysis in duplicate, the ratios were not averaged to increase the accuracy of the fit. Errors in normalized peak intensity changes (A, B, D) and normalized chemical shift changes (C) were estimated from standard deviations when averaging values observed for different residues (see text). The largest calculated standard deviations are 0.04 (A), 0.03 (B), 0.03 (C), and 0.04 (D).

the sequence, the α-helical regions (E, F, G, and H helices) are perturbed to a greater extent than other residues, especially at the end of the H helix.

Titration of CTnC·2Ca^{2+} with TnI$_{96-115}$. Figure 3B depicts the TnI_{96-115}-induced backbone amide ^{1}HN, ^{15}N chemical shift changes for CTnC·$2Ca^{2+}$. Unlike Ca^{2+} binding to CTnC and Rp40 binding to CTnC·$2Ca^{2+}$, TnI_{96-115} binding to CTnC·$2Ca^{2+}$ occurs with fast exchange kinetics on the NMR time scale. Thus, progressive shifting of the resonances is observed, and the chemical shifts at every titration point correspond to the weighed average of the peptide-free and -bound species. Some residues that undergo relatively large chemical shift changes and do not overlap with other resonances are identified in Figure 3B. When the chemical shift changes of E95, F105, E132, I134, K156, and G160 are normalized and plotted against the $[TnI_{96-115}]_{total}$:$[CTnC{\cdot}2Ca^{2+}]_{total}$ ratio, similar curves are obtained. Figure 2C shows the averaged normalized chemical shift changes of the six chosen residues. Curve fitting to the equation:

$$CTnC{\cdot}2Ca^{2+} + TnI_{96-115} \rightleftharpoons CTnC{\cdot}2Ca^{2+}{\cdot}TnI_{96-115} \quad (4)$$

yields a dissociation constant $K_D = 47 \pm 7$ μM, which is 24 times larger than that observed for Rp40. Several studies have examined the binding affinities of TnI_{96-115} and $TnI_{104-115}$ with intact or isolated CTnC (see refs *28*, *32*, *63*, *64* and references cited therein). The reported binding affinities are in good agreement with the value reported here (47 ± 7 μM). The total chemical shift changes calculated using eq 3 are plotted against the CTnC sequence (Figure 4B). Compared to Rp40-induced chemical shift changes in CTnC·$2Ca^{2+}$ (Figure 4A), similar patterns for TnI_{96-115}-induced changes are observed. The changes occur along the entire sequence, but are relatively larger in the α-helical regions (E, F, G, and H helices). These results indicate that TnI_{96-115} may compete with Rp40 for a similar location on CTnC.

Competitive Binding: (A) Titration of CTnC·2Ca^{2+}·TnI$_{96-115}$ with Rp40. Following the titration of CTnC·$2Ca^{2+}$ with TnI_{96-115}, Rp40 was titrated into the CTnC·TnI_{96-115}·$2Ca^{2+}$ complex. The 2D-{^{1}H, ^{15}N}-HSQC NMR spectrum of CTnC·$2Ca^{2+}$·TnI_{96-115} exhibited changes with the first addition of Rp40. New peaks exhibiting the same chemical shifts as CTnC·$2Ca^{2+}$·Rp40 emerged and gained in intensity as the ratio of Rp40:CTnC·$2Ca^{2+}$·TnI_{96-115} increased, whereas the peaks corresponding to CTnC·$2Ca^{2+}$·TnI_{96-115} diminished

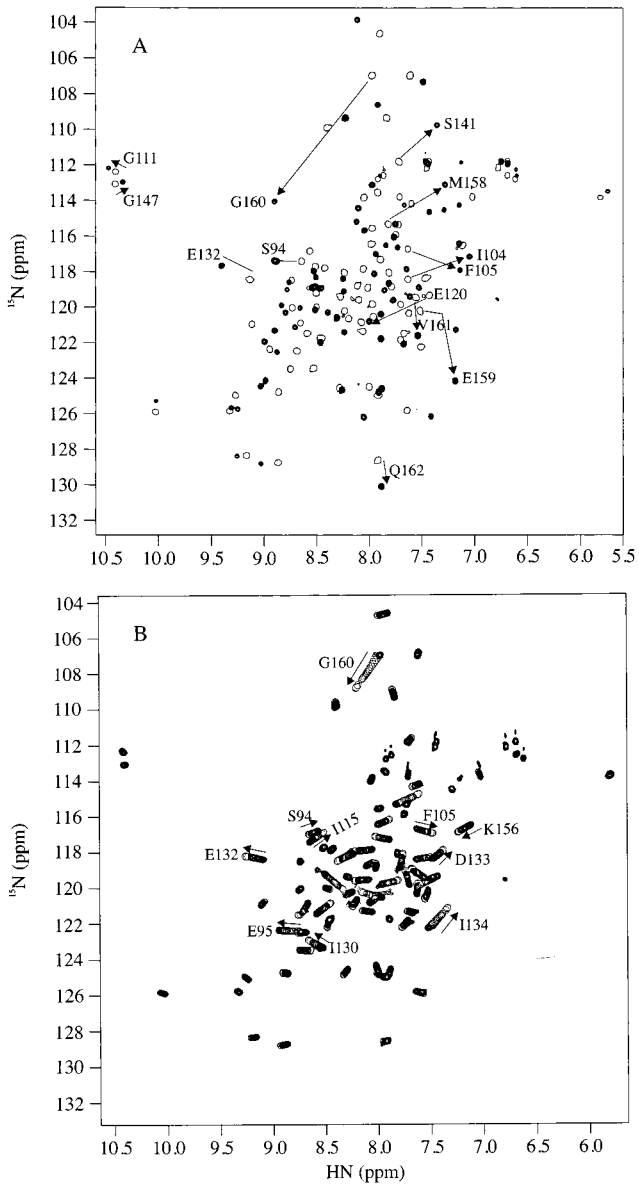

FIGURE 3: 500 MHz 2D-{^{1}H, ^{15}N}-HSQC NMR spectrum acquired during the titration of CTnC·2Ca^{2+} with (A) Rp40 and (B) TnI_{96-115}. In (A), the 2D-{^{1}H,^{15}N}-HSQC NMR spectrum of CTnC·2Ca^{2+} is shown in single contours, whereas peaks associated with complex formation with Rp40:CTnC at a 1:1 ratio are shown in multiple contours. In (B), the 2D-{^{1}H,^{15}N}-HSQC NMR spectrum of CTnC·2Ca^{2+} is shown in multiple contours, whereas peak changes upon each TnI_{96-115} addition are shown in single contours. In both panels, the directions of the chemical shift changes for some residues undergoing large perturbations are indicated by an arrow.

in intensity. Rp40 was added until no further changes in the spectrum were observed. The final 2D-{^{1}H, ^{15}N}-HSQC NMR spectrum of CTnC·2Ca^{2+}·TnI_{96-115}·Rp40 (data not shown) is identical to that of CTnC·2Ca^{2+}·Rp40 (Figure 3A). Following the same data treatment procedures as in the titration of CTnC·2Ca^{2+} with Rp40, a K_D of 3 ± 1 μM is obtained (Figure 2D), which is identical to the affinity of Rp40 binding to CTnC·2Ca^{2+} (Figure 2B). These results suggest Rp40 can displace TnI_{96-115} completely for CTnC·2Ca^{2+} and its affinity for CTnC·2Ca^{2+} is unaffected by the presence of TnI_{96-115} within experimental error. Additional evidence for the displacement of TnI_{96-115} was provided from 1D ^{1}H NMR spectra recorded during the titration. Figure 5 shows shifting of TnI_{96-115} resonances from aromatic side chains toward the free peptide chemical shifts in solution as the addition of Rp40 displaces TnI_{96-115} from the complex.

Competitive Binding: (B) Titration of CTnC·2Ca^{2+}·Rp40 with TnI_{96-115}. Following the titration of CTnC·2Ca^{2+} with Rp40, TnI_{96-115} was added to the complex. No changes in the 2D-{^{1}H, ^{15}N}-HSQC NMR spectrum of CTnC·2Ca^{2+}·Rp40 were observed, even at a TnI_{96-115}:Rp40 ratio of 10:1. It is obvious that TnI_{96-115} cannot bind to the complex of CTnC·2Ca^{2+}·Rp40 in any fashion. Thus, it cannot displace Rp40 from CTnC·2Ca^{2+}.

DISCUSSION

When TnC is anchored to the thin filament by its C-terminal domain, the rapid association of Ca^{2+} with the N-terminal Ca^{2+}-specific regulatory sites of TnC initiates muscle contraction. In the past few years, we have been successful in determining the solution structures of skeletal and cardiac TnC in various states (*9*, *10*, *24*, *35*, *65*−*67*). These structures, together with Ca^{2+} and peptide binding studies (*18*, *19*, *23*, *36*), have allowed us to dissect the mechanism and energetics of Ca^{2+}-induced structural changes in the regulatory domain of TnC and subsequent interactions with TnI. In this report, we have focused on the structural domain of TnC and studied in detail Ca^{2+} and TnI peptide binding to CTnC by using 2D-{^{1}H, ^{15}N}-HSQC NMR spectroscopy.

Previously, fluorescence and far-UV CD spectroscopy (*68*) have been used to examine Ca^{2+} binding to CTnC (residues 88−162). Pearlstone and Smillie (*28*, *69*) have applied the same spectroscopic techniques to the measurement of binding affinities of TnI_{96-116}, $TnI_{104-116}$, and TnI_{96-148} to CTnC. Changes in fluorescence or CD spectra reflect global conformational changes accompanying Ca^{2+} or peptide binding to CTnC, but do not reveal details at the atomic level that can be used to elucidate the detailed binding mechanism. Shaw and Sykes (*70*−*73*) demonstrated the power of ^{1}H NMR spectroscopy in determining the stoichiometry and binding of Ca^{2+} to synthetic peptide homo- and heterodimeric TnC domains. 2D-{^{1}H, ^{15}N}-HSQC NMR spectroscopy is an even more powerful diagnostic tool as chemical shift overlap encountered in ^{1}H NMR spectra can be overcome (*18*, *23*, *24*, *35*, *36*).

The amide NH chemical shifts shown in the 2D-{^{1}H, ^{15}N}-HSQC NMR spectrum of CTnC·apo (Figure 1A) reflect the characteristics of a "random coil" peptide whereas the dispersion of amide signals seen for CTnC·2Ca^{2+} (Figure 1B) is more typical of a structured protein. Chemical shift changes observed upon Ca^{2+} binding to CTnC allow monitoring of Ca^{2+}-induced "folding" of this domain. For example, the appearance of Gly^{111} and Gly^{147} at ~10.5 ppm (Figure 1B) indicates that the two glycine amide protons are involved in important EF-hand hydrogen bonding interactions, as observed in X-ray structures of TnC [see review by Strynadka (*74*)]. Although the 2D-{^{1}H,^{15}N}-HSQC NMR spectrum of CTnC·apo is indicative of a predominant "random coil" conformation, previous far-UV CD studies of CTnC·apo suggested a small fraction of preformed α-helical content (*68*). This suggests that CTnC·apo may not be completely "random coil" but contains some partial structures.

Fredricksen and Swenson (*75*) examined the relationship between stability and function for isolated N- and C-domains

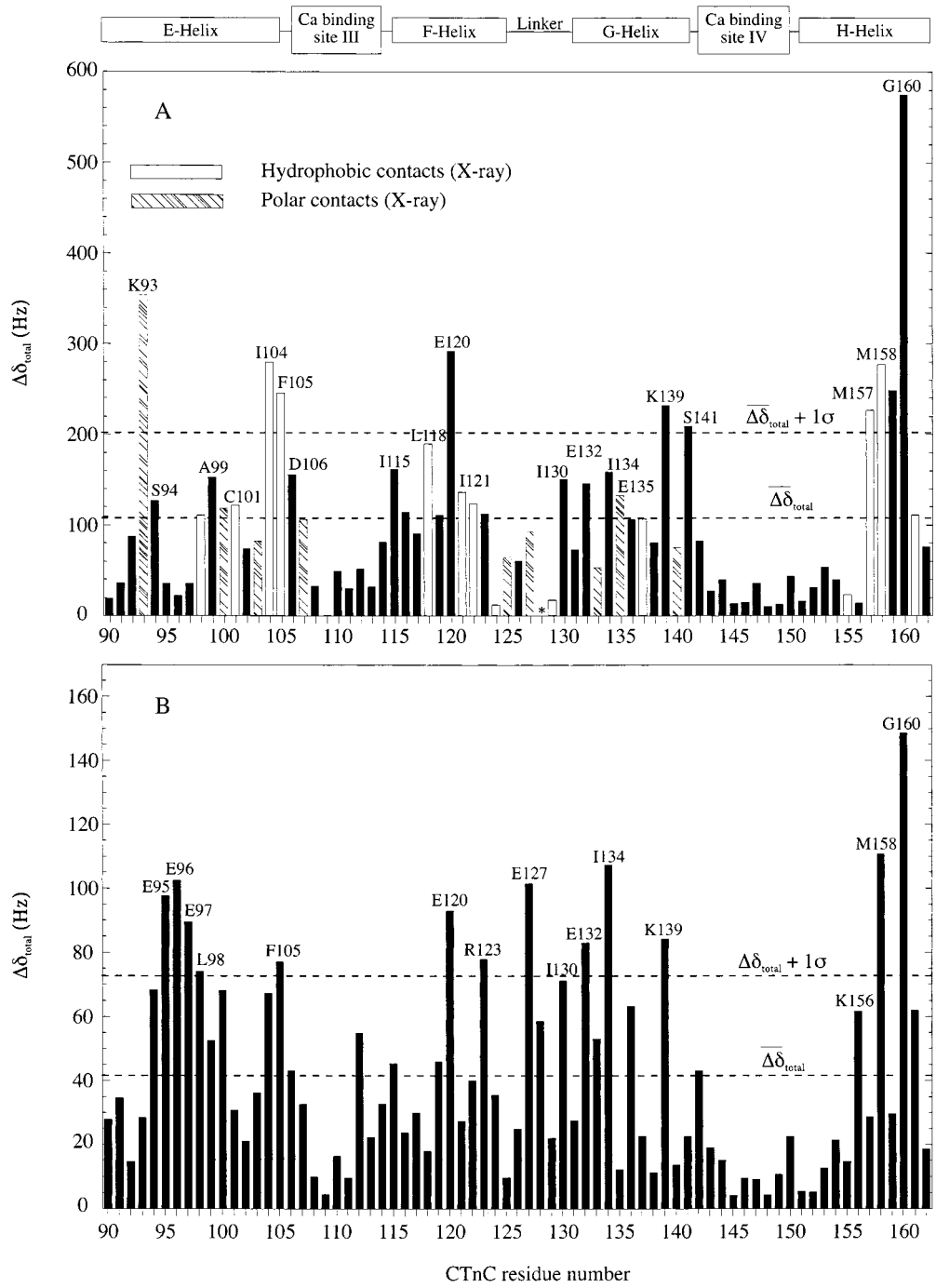

FIGURE 4: CTnC·2Ca^{2+} backbone amide chemical shift changes upon (A) Rp40 and (B) TnI$_{96-115}$ binding. The total chemical shift change ($\Delta\delta_{total}$) for each residue was obtained using eq 3. The two dashed lines indicate the mean chemical shift change and the mean chemical shift plus one standard deviation. (*) In (A), the backbone amide resonance of H128 could not be identified in the 2D-{^{1}H,^{15}N}-HSQC NMR spectrum of CTnC·2Ca^{2+}·Rp40. Residues identified by Vassylyev et al. (*53*) making hydrophobic (white bars) and polar contacts (gray bars) to CTnC are specifically colored.

of TnC. It was demonstrated that while Ca^{2+} affinity and cooperativity are higher for the C-domain, it is unstructured in the apo state, whereas the N-domain has lower Ca^{2+} affinity but a stable, folded apo state. This agrees with our results for NTnC (*18*) and CTnC (this study). The high positive cooperativity and high affinity for Ca^{2+} of paired sites III/IV of CTnC preclude a regulatory role in muscle regulation. On the other hand, the stepwise binding of Ca^{2+} to site II followed by binding to site I to NTnC allows this domain to play a regulatory role, with Ca^{2+} affinities in an appropriate physiological concentration range, and rapid enough Ca^{2+} dissociation to be kinetically competent (see discussions in references *19* and *65*).

The interaction of CTnC·2Ca^{2+} with TnI is important to its structural function. Both Rp40 and TnI$_{96-115}$ are implicated in binding to CTnC·2Ca^{2+} [see Tripet et al. (*30*) and references cited therein]. There is controversy surrounding the binding of these two regions of TnI to TnC, particularly because of the observation that the N-terminal residues of TnI interact with CTnC (*43*), and that Rp40 can effectively compete with TnI or TnI$_{104-115}$ for binding to TnC (54). Two models have been proposed for the interaction of the

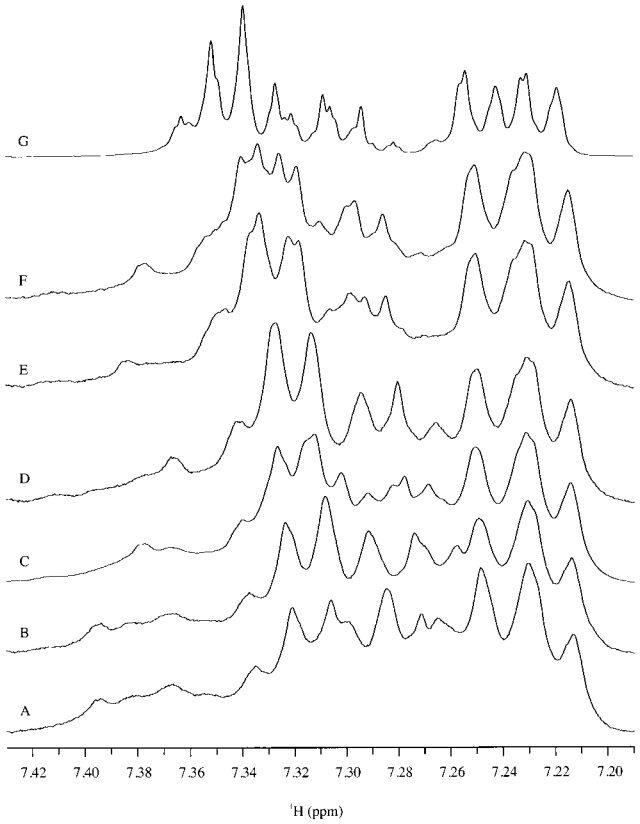

FIGURE 5: 500 MHz ^{1}H NMR spectra of CTnC·2Ca^{2+}·TnI_{96-115} at (A) 0, (B) 0.08, (C) 0.17, (D) 0.27, (E) 0.39, and (F) 0.61 Rp40: TnI_{96-115} ratios and TnI_{96-115} free in solution (G).

N-terminal region of TnI with CTnC. The first one suggests that Rp40 and TnI_{96-115} share overlapping binding sites on CTnC, which are alternately occupied by either one or the other depending on Ca^{2+}-dependent interactions between NTnC and TnI (*30*, *36*, *39*). On the other hand, the second model has TnI_{1-47} specifically involved in binding to the hydrophobic patch within CTnC, regardless of Ca^{2+}-dependent interactions between NTnC and TnI (*53*). The competitive binding of Rp40 and TnI_{96-115} presented here shows that both regions of TnI bind to similar sites within the C-domain of TnC but that Rp40 can displace TnI_{96-115} completely. Thus, either the inhibitory region is not bound to the structural domain of TnC in intact muscle, or other Ca^{2+}-dependent interactions between TnI and TnC, possibly also involving TnT and actin, are necessary to help displace Rp40.

The Rp40- and TnI_{96-115}-induced chemical shift changes for the backbone amides of CTnC·2Ca^{2+} can be used to identify the location of the binding sites for the respective peptides. Chemical shift mapping has proven to be a convenient way to locate target binding sites on proteins. A recent paper by Biekofsky et al. (*21*) has discussed in detail the potential of using ^{15}N chemical shifts as probes for monitoring individual Ca^{2+} coordination site in EF-hand proteins. Previously, we successfully applied chemical shift mapping to identify binding sites of $TnI_{115-131}$ and TnI_{96-148} on NTnC (*23*, *35*) and cardiac $TnI_{147-163}$ on cardiac NTnC (*24*).

Molecular surfaces of CTnC mapping out total chemical shift changes upon binding of TnI_{96-115} and Rp40 are shown in Figure 6. To reflect the difference in extent of total chemical shift changes for both peptides, the surfaces were colored on a color gradient scale from white to red (see color bar in Figure 6). The X-ray structure determined for TnC·2Ca^{2+}·TnI_{1-47} (*53*) and the Ngai model of CTnC·TnI_{96-115} (*27*), which includes the C-domain of the X-ray structure determined for whole TnC·4Ca^{2+} by James et al. (*7*), were used to compare the perturbation sites caused by the binding of Rp40 and TnI_{96-115}, respectively.

In Figure 6B, the TnC residues whose backbone amide chemical shifts are perturbed match similar regions where Rp40−CTnC contacts were observed in the X-ray structure of TnC·2Ca^{2+}·TnI_{1-47} (*53*). Corresponding residues for the C-domain of cardiac TnC were also identified in the interaction with cardiac TnI_{33-80} (*37*). Residues that undergo large backbone amide chemical shift changes are mostly hydrophobic and mainly located in the hydrophobic patch of CTnC·2Ca^{2+}, indicating that Rp40 binds to this particular region. This is consistent with the X-ray structure (*53*), in which Met^{21} of Rp40 makes contacts deep in the hydrophobic patch of TnC and was suggested to be a key residue in anchoring Rp40. Two other regions identified in red, located in the C- and N-termini of TnC, are also found to be strongly influenced by Rp40 binding (Figure 6B). ^{15}N T_2 NMR relaxation studies of the CTnC·2Ca^{2+}·Rp40 complex have revealed that Rp40 restricts the flexibility of residues located in these hinge and terminal regions compared to CTnC·2Ca^{2+} (P. Mercier et al., manuscript in preparation).

In the case of TnI_{96-115}, no high-resolution structure of this peptide bound to the C-domain of CTnC is available, so we have used the model of Ngai et al. (*27*) showing the complex between CTnC and the shorter $TnI_{104-115}$ peptide. A comparison between Figure 4A,B and Figure 6B,C shows that the TnI_{96-115} inhibitory peptide perturbs the local environment of some of the same CTnC residues involved in binding Rp40, reinforcing the hypothesis of similar binding sites. The fact that Rp40 displaces TnI_{96-115} also implies at least partially overlapping sites. The CTnC·2Ca^{2+} amide chemical shift changes induced by TnI_{96-115} are similarly distributed as in the case of Rp40, with perturbations of residues located in helical regions (helices E, F, G, and H). Residues undergoing the largest chemical shift changes include Ser^{94}, Phe^{105}, Glu^{120}, Lys^{139}, Met^{158}, and Gly^{160}, in both cases. However, as judged by the magnitude of chemical shift changes (see Figure 4), the perturbations induced by TnI_{96-115} are much weaker. A close examination of the chemical shift data suggests key differences between Rp40 and TnI_{96-115} binding. The CTnC chemical shift changes (Figure 4B) imply that six charged residues (Glu^{95}, Glu^{96}, Glu^{97}, Glu^{120}, Glu^{127}, Glu^{132}, Arg^{123}, and Lys^{139}) likely participate in the binding of TnI_{96-115}. Thus, the nature of the interaction with TnC is more electrostatic for TnI_{96-115}, as opposed to more hydrophobic for Rp40, which is also consistent with the relatively high percentage of charged residues in TnI_{96-115}.

Previous NMR structural studies based on transferred NOE experiments by Campbell et al. reported that $TnI_{104-115}$ adopts an amphiphilic helix-like structure, distorted at the center around the two Pro residues (*33*). However, recent NMR and CD results indicate that TnI_{96-115} remains in an extended form upon binding to TnC, with a possible bend at Gly^{104} (*39*). The eight residue difference between $TnI_{104-115}$ and TnI_{96-115} might explain the differences in secondary structure observed for these two peptides. The shorter TnI peptide may bind slightly differently, whereas the extensive TnI_{96-115} contacts identified in this report suggest a more extended structure for the longer peptide.

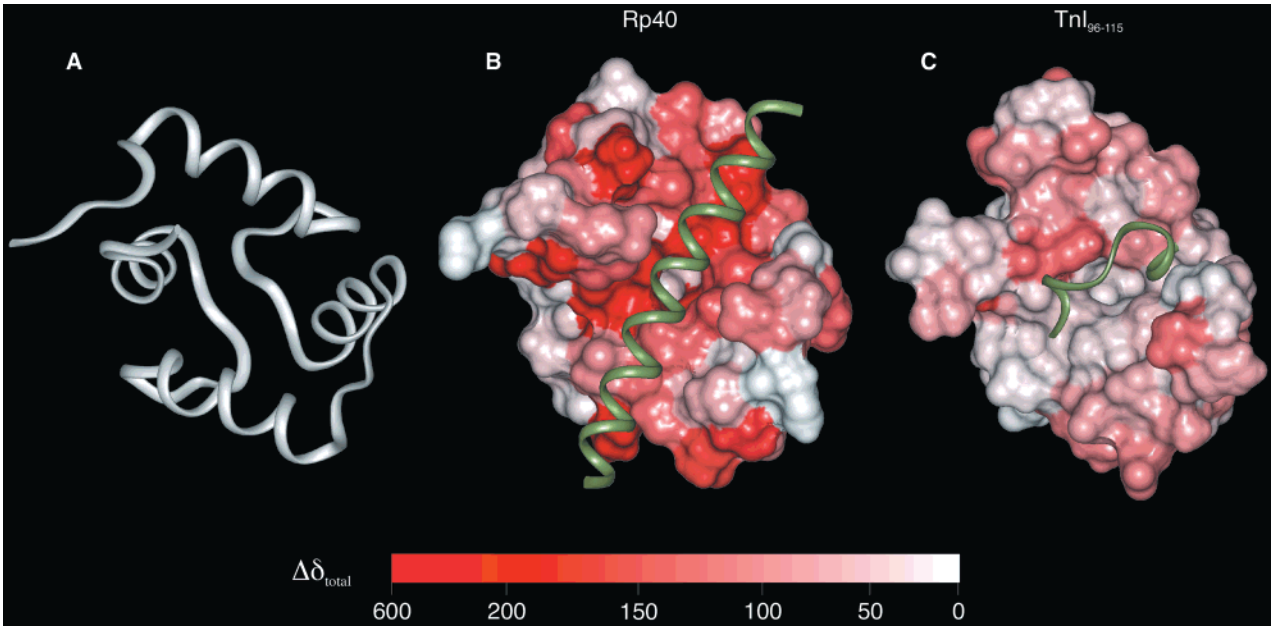

FIGURE 6: Molecular surface of CTnC in complex with (B) Rp40 and (C) TnI_{96-115}. The orientation of the protein backbone is shown as a ribbon diagram in (A). To show the difference in the extent of the total chemical shift changes ($\Delta\delta_{total}$) between Rp40 and TnI_{96-115} binding (Figure 4), the surfaces were colored using a color gradient (from white to red: see color bar). Residues undergoing total chemical shift changes larger than 200 Hz (which corresponds to $\approx\overline{\Delta\delta_{total}} + 1\sigma$ with Rp40) were colored pure red. Smaller total chemical shift changes were colored on a linear scale. The X-ray structure of CTnC·TnI_{1-47} (*53*) and model of CTnC·TnI_{96-115} (*27*) were used in (A) and (B), respectively.

A recent structure of cNTnC·$cTnI_{147-163}$·$2Ca^{2+}$ shows that $cTnI_{147-163}$ is helical from residues 151 to 156. At the end N-terminal of the helix, the peptide makes a turn which allows Ile^{148} to make hydrophobic contacts with cardiac NTnC, placing Arg^{147} in a position where an interaction with the acidic residues of the C-helix is possible. Based on chemical shift mapping results, we believe TnI_{96-115} may also adopt a similar turn to avoid contact with the H helix and interact with the G helix. Only minor rearrangement of the location of TnI_{96-115} relative to $TnI_{104-115}$ would be necessary to satisfy the contact region located between the E and H helices on TnC (Figure 6C). Thus, even though TnI_{96-115} and Rp40 share common epitopes on TnC, the two peptides may have different structures and orientations in the bound form. Together with previous structural data, our results suggest that Rp40 makes several contacts within the hydrophobic patch, while TnI_{96-115} may bind across the top of the hydrophobic patch. Thus, both electrostatic and hydrophobic interactions may be involved in TnI_{96-115} binding to CTnC, while hydrophobic interactions dominate in the case of Rp40.

In this paper, 2D-{^{1}H,^{15}N}-HSQC NMR spectroscopy was used to demonstrate that 2 equiv of Ca^{2+} is required for folding CTnC. Unlike the stepwise binding mechanism observed for NTnC, CTnC binds Ca^{2+} with high positive cooperativity and high affinity. Rp40 and TnI_{96-115} were shown to bind to CTnC·$2Ca^{2+}$ with dissociation constants of 2 ± 1 and 47 ± 7 μM, respectively. Residues of CTnC that are perturbed by the binding of Rp40 or TnI_{96-115} were identified using chemical shift mapping. The chemical shift changes suggest that Rp40 binds to the hydrophobic pocket of CTnC·$2Ca^{2+}$, while TnI_{96-115} binds across the top of the hydrophobic pocket. The measured K_D's quantitatively explain the displacement of TnI_{96-115} from CTnC·$2Ca^{2+}$ by Rp40. In the Tripet et al. (*30*) model, the binding of the inhibitory region of TnI to the C-terminal domain of TnC is important in the release of actomyosin ATPase inhibition. Our results imply that for this to be possible, Ca^{2+}-dependent interactions between TnC and other regions of TnI, or other components of the thin filament, must be involved. The results of peptide studies with short peptides such as TnI_{96-115} must always be interpreted with caution. There may be other interaction sites that are missing, or the binding of TnI_{96-115} to the target protein is in a nonphysiologically relevant site.

ACKNOWLEDGMENT

We are indebted to Dr. Ryan McKay and Dr. Leo Spyracopoulos for insightful discussions and to Mr. Robert Boyko for his assistance with the curve-fitting program. We thank Mr. David Corson for preparation of the CTnC protein and Mr. Gerry McQuaid for maintenance of the spectrometers.

REFERENCES

1. Leavis, P. C., and Gergely, J. (1984) *CRC Crit. Rev. Biochem. 16*, 235−305.
2. Zot, A. S., and Potter, J. D. (1987) *Annu. Rev. Biophys. Biophys. Chem. 16*, 535−559.
3. Grabarek, Z., Tao, T., and Gergely, J. (1992) *J. Muscle Res. Cell Motil. 13*, 383−393.
4. Farah, C. S., and Reinach, F. C. (1995) *FASEB J. 9*, 755−767.
5. Tobacman, L. S. (1996) *Annu. Rev. Physiol. 58*, 447−481.
6. Squire, J. M., and Morris, E. P. (1998) *FASEB J. 12*, 761−771.
7. Herzberg, O., and James, M. N. G. (1988) *J. Mol. Biol. 203*, 761−779.
8. Satyshur, K. A., Rao, S. T., Pyzalska, D., Drendal, W., Greaser, M., and Sundaralingam, M. (1988) *J. Biol. Chem. 263*, 1628−1647.
9. Slupsky, C. M., and Sykes, B. D. (1995) *Biochemistry 34*, 15953−15964.
10. Gagné, S. M., Tsuda, S., Li, M. X., Smillie, L. B., and Sykes, B. D. (1995) *Nat. Struct. Biol. 2*, 784−789.

11. Houdusse, A., Love, M. L., Dominguez, R., Grabarek, Z., and Cohen, C. (1997) *Structure 5*, 1695−1711.
12. Leavis, P. C., Rosenfeld, S. S., and Gergely, J. (1978) *J. Biol. Chem. 253*, 5452−5459.
13. Potter, J. D., and Gergely, J. (1975) *J. Biol. Chem. 250*, 4628−4633.
14. Szczesna, D., Guzman, G., Miller, T., Zhao, J., Farokhi, K., Ellemberger, H., and Potter, J. D. (1996) *J. Biol. Chem. 271*, 8381−8386.
15. Gergely, J. (1998) *Adv. Exp. Med. Biol. 453*, 169−176.
16. Gagné, S. M., Li, M. X., McKay, R. T., and Sykes, B. D. (1998) *Biochem. Cell Biol. 76*, 301−312.
17. Rao, S. T., Satyshur, K. A., Greaser, M. L., and Sundaralingam, M. (1996) *Acta Crystallogr., Sect. D 52*, 916−922.
18. Li, M. X., Gagné, S. M., Tsuda, S., Kay, C. M., Smillie, L. B., and Sykes, B. D. (1995) *Biochemistry 34*, 8330−8340.
19. Li, M. X., Gagné, S. M., Spyracopoulos, L., Kloks, C. P. A. M., Audette, G., Chandra, M., Solaro, R. J., Smillie, L. B., and Sykes, B. D. (1997) *Biochemistry 36*, 12519−12525.
20. Evenas, J., Thulin, E., Malmendal, A., Forsén, S., and Carlstrom, G. (1997) *Biochemistry 36*, 3448−3457.
21. Biekofsky, R. R., Martin, S. R., Browne, J. P., Bayley, P. M., and Feeney, J. (1998) *Biochemistry 37*, 7617−7629.
22. Wimberly, B., Thulin, E., and Chazin, W. J. (1995) *Protein Sci. 4*, 1045−1055.
23. McKay, R. T., Tripet, B. P., Hodges, R. S., and Sykes, B. D. (1997) *J. Biol. Chem. 272*, 28494−28500.
24. Li, M. X., Spyracopoulos, L., and Sykes, B. D. (1999) *Biochemistry 38*, 8289−8298.
25. Olah, G. A., Rokop, S. E., Wang, C.-L. A., Blechner, S. L., and Trewhella, J. (1994) *Biochemistry 33*, 8233−8239.
26. Olah, G. A., and Trewhella, J. (1994) *Biochemistry 33*, 12800−12806.
27. Ngai, S.-M., Sönnichsen, F. D., and Hodges, R. S. (1994) *J. Biol. Chem. 269*, 2165−2172.
28. Pearlstone, J. R., and Smillie, L. B. (1995) *Biochemistry 34*, 6932−6940.
29. Pearlstone, J. R., and Smillie, L. B. (1997) *Biophys. J. 72*, A331.
30. Tripet, B. P., Van Eyk, J. E., and Hodges, R. S. (1997) *J. Mol. Biol. 271*, 728−750.
31. Campbell, A. P., and Sykes, B. D. (1991) *J. Mol. Biol. 222*, 405−421.
32. Campbell, A. P., Cachia, P. J., and Sykes, B. D. (1991) *Biochem. Cell Biol. 69*, 674−681.
33. Campbell, A. P., Van Eyk, J. E., Hodges, R. S., and Sykes, B. D. (1992) *Biochim. Biophys. Acta 1160*, 35−54.
34. Slupsky, C. M., Shaw, G. S., Campbell, A. P., and Sykes, B. D. (1992) *Protein Sci. 1*, 1595−1603.
35. McKay, R. T., Pearlstone, J. R., Corson, D. C., Gagné, S. M., Smillie, L. B., and Sykes, B. D. (1998) *Biochemistry 37*, 12419−12430.
36. McKay, R. T., Tripet, B. P., Pearlstone, J. R., Smillie, L. B., and Sykes, B. D. (1999) *Biochemistry 38*, 5478−5489.
37. Gasmi-Seabrook, G., Howarth, J. W., Finley, N., Abusamhadneh, E., Gaponenko, V., Brito, R. M., Solaro, R. J., and Rosevear, P. R. (1999) *Biochemistry 38*, 8313−8322.
38. Gaponenko, V., Abusamhadneh, E., Abbott, M. B., Finley, N., Gasmi-Seabrook, G., Solaro, R. J., Rance, M., and Rosevear, P. R. (1999) *J. Biol. Chem. 274*, 16681−16684.
39. Hernández, G., Blumenthal, D. K., Kennedy, M. A., Unkefer, C. J., and Trewhella, J. (1999) *Biochemistry 38*, 6911−6917.
40. Syska, H., Wilkinson, J. M., Grand, R. J. A., and Perry, S. V. (1976) *Biochem. J. 153*, 375−387.
41. Talbot, J. A., and Hodges, R. S. (1981) *J. Biol. Chem. 256*, 2798−2802.
42. Van Eyk, J. E., and Hodges, R. S. (1988) *J. Biol. Chem. 263*, 1726−1732.
43. Farah, C. S., Miyamoto, C. A., Ramos, C. H. I., da Silva, A. C. R., Quaggio, R. B., Fujimori, K., Smillie, L. B., and Reinach, F. C. (1994) *J. Biol. Chem. 269*, 5230−5240.
44. Kobayashi, T., Tao, T., Grabarek, Z., Gergely, J., and Collins, J. H. (1991) *J. Biol. Chem. 266*, 13746−13751.
45. Kobayashi, T., Tao, T., Gergely, J., and Collins, J. H. (1994) *J. Biol. Chem. 269*, 5725−5729.
46. Kobayashi, T., Grabarek, Z., Gergely, J., and Collins, J. H. (1995) *Biochemistry 34*, 10946−10952.
47. Kobayashi, T., Leavis, P. C., and Collins, J. H. (1996) *Biochim. Biophys. Acta 1294*, 25−30.
48. Kobayashi, T., Zhao, X., Wade, R., and Collins, J. H. (1999) *Biochim. Biophys. Acta 1430*, 214−221.
49. Leszyk, J., Collins, J. H., Leavis, P. C., and Tao, T. (1988) *Biochemistry 27*, 6983−6987.
50. Leszyk, J., Grabarek, Z., Gergely, J., and Collins, J. H. (1990) *Biochemistry 29*, 299−304.
51. Blechner, S. L., Olah, G. A., Strynadka, N. C., Hodges, R. S., and Trewhella, J. (1992) *Biochemistry 31*, 11326−11334.
52. Stone, D. B., Timmins, P. A., Schneider, D. K., Krylova, I., Ramos, C. H. I., Reinach, F. C., and Mendelson, R. A. (1998) *J. Mol. Biol. 281*, 689−704.
53. Vassylyev, D. G., Takeda, S., Wakatsuki, S., Maeda, K., and Maeda, Y. (1998) *Proc. Natl. Acad. Sci. U.S.A. 95*, 4847−4852.
54. Ngai, S.-M., and Hodges, R. S. (1992) *J. Biol. Chem. 267*, 15715−15720.
55. Ramos, C. H. I. (1999) *J. Biol. Chem. 274*, 18189−18195.
56. Gagné, S. M., Tsuda, S., Li, M. X., Chandra, M., Smillie, L. B., and Sykes, B. D. (1994) *Protein Sci. 3*, 1961−1974.
57. Kay, L. E., Keifer, P., and Saarinen, T. (1992) *J. Am. Chem. Soc. 114*, 10663−10665.
58. Zhang, O., Kay, L. E., Olivier, J. P., and Forman-Kay, J. D. (1994) *J. Biomol. NMR 4*, 845−858.
59. Delaglio, F., Grzesiek, S., Vuister, G. W., Zhu, G., Pfeifer, J., and Bax, A. (1995) *J. Biomol. NMR 6*, 277−293.
60. Wüthrich, K. (1986) *NMR of proteins and nucleic acids*, John Wiley & Sons, New York.
61. Wishart, D. S., Sykes, B. D., and Richards, F. M. (1991) *J. Mol. Biol. 222*, 311−333.
62. Ferguson-Miller, S., and Koppenol, W. H. (1981) *Trends Biochem. Sci. 6*, IV−VII.
63. Cachia, P. J., Van Eyk, J., Ingraham, R. H., McCubbin, W. D., Kay, C. M., and Hodges, R. S. (1986) *Biochemistry 25*, 3553−3562.
64. Swenson, C. A., and Fredricksen, R. S. (1992) *Biochemistry 31*, 3420−3429.
65. Gagné, S. M., Li, M. X., and Sykes, B. D. (1997) *Biochemistry 36*, 4386-4392.
66. Sia, S. K., Li, M. X., Spyracopoulos, L., Gagné, S. M., Liu, W., Putkey, J. A., and Sykes, B. D. (1997) *J. Biol. Chem. 272*, 18216−18221.
67. Spyracopoulos, L., Li, M. X., Sia, S. K., Gagné, S. M., Chandra, M., Solaro, R. J., and Sykes, B. D. (1997) *Biochemistry 36*, 12138−12146.
68. Li, M. X., Chandra, M., Pearlstone, J. R., Racher, K. I., Trigo-Gonzalez, G., Borgford, T., Kay, C. M., and Smillie, L. B. (1994) *Biochemistry 33*, 917−925.
69. Pearlstone, J. R., Sykes, B. D., and Smillie, L. B. (1997) *Biochemistry 36*, 7601−7606.
70. Shaw, G. S., Hodges, R. S., and Sykes, B. D. (1990) *Science 249*, 280−283.
71. Shaw, G. S., Golden, L. F., Hodges, R. S., and Sykes, B. D. (1991) *J. Am. Chem. Soc. 113*, 5557−5562.
72. Shaw, G. S., Hodges, R. S., and Sykes, B. D. (1991) *Biochemistry 30*, 8339−8347.
73. Shaw, G. S., Hodges, R. S., and Sykes, B. D. (1992) *Biopolymers 32*, 391−397.
74. Strynadka, N. C., and James, M. N. G. (1989) *Annu. Rev. Biochem. 58*, 951−998.
75. Fredricksen, S. R., and Swenson, C. A. (1996) *Biochemistry 35*, 14012−14026.

BI992579N